

Perovskites

How to cite: *Angew. Chem. Int. Ed.* **2021**, 60, 23735–23742

International Edition: doi.org/10.1002/anie.202108495

German Edition: doi.org/10.1002/ange.202108495

Interfacial Linkage and Carbon Encapsulation Enable Full Solution-Printed Perovskite Photovoltaics with Prolonged Lifespan

Tian Tian, Jun-Xing Zhong, Meifang Yang, Wenhui Feng, Chengxi Zhang, Wenjing Zhang, Yaser. Abdi, Lianzhou Wang,* Bing-Xin Lei,* and Wu-Qiang Wu*

Abstract: Simplified perovskite solar cells (PSCs) were fabricated with the perovskite layer sandwiched and encapsulated between carbon-based electron transport layer (ETL) and counter electrode (CE) by a fully blade-coated process. A self-assembled monolayer of amphiphilic silane (AS) molecules on transparent conducting oxide (TCO) substrate appeals to the fullerene ETL deposition and preserves its integrity against the solvent damage. The AS serves as a “molecular glue” to strengthen the adhesion toughness at the TCO/ETL interface via robust chemical interaction and bonding, facilitating the interfacial charge extraction, increasing PCEs by 77% and reducing hysteresis. A PCE of 18.64% was achieved for the fully printed devices, one of the highest reported for carbon-based PSCs. AS-assisted interfacial linkage and carbon-material-assisted self-encapsulation enhance the stability of the PSCs, which did not experience performance degradation when stored at ambient conditions for over 3000 h.

Introduction

Over the past decade, perovskite solar cells (PSCs) have attracted a great deal of research interest and effort owing to their low cost and high efficiency.^[1–10] To date, the power conversion efficiencies (PCEs) of single-junction PSCs have been elevated to a certified value of 25.5%,^[11] comparable to silicon-based photovoltaic counterparts. The next step to boost the commercialization of this emerging perovskite photovoltaic technology is to further simplify the fabrication procedure, lower the fabrication cost and improve the device stability, together with promoting scalability.^[1,12] The solution processability of the halide perovskite layer has endowed the perovskite photovoltaics a promising prospect towards roll-to-roll manufacturing in a low-cost manner, if other functional

layers, namely, the charge transport layer (CTL) and counter electrode (CE), can also be fabricated via a full solution process. Full solution-processed PSC multilayer stack is still particularly challenging because the deposition of one layer will unintentionally damage the underlying layer to some extent even though the orthometric solvent system has been carefully considered.

Among various kinds of PSCs, all carbon-based PSCs with the perovskite layer sandwiched between fullerene CTL and carbon CE seem to be the most ideal option for balancing the cost-efficiency-stability triangle, because carbon materials inherently have the fascinating characteristics of high stability, low cost, hydrophobicity, high conductivity, and excellent heat dissipation capability.^[13–15] It is well-known that the conventional PSCs normally suffer from ion diffusion from the perovskite to the metal electrodes (i.e. gold (Au) and silver (Ag)), resulting in irreversible electrode corrosion, material decomposition and performance degradation. In addition, the metal ions can also migrate to the perovskite layer, which would create energy trap states and cause unexpected non-radiative recombination.^[16] In contrast, the carbon-based electrode is inert to ion migration, which is beneficial to improve the operational stability of PSCs.^[17–21] For now, a variety of carbon materials, such as fullerene and its derivatives, carbon black, graphite, graphene, carbon nanotubes, etc., have been employed in PSCs, either as electron transport layer (ETL), CE, or interfacial modification layer.^[18–20] Typically, the fullerene (i.e. C₆₀) and its derivatives have been regarded as one of the most promising alternative ETL candidates to be used in high-performance PSCs.^[18–20,22] The C₆₀ ETL is found to be advantageous in terms of low-temperature processability, more matched energy level alignment with perovskites and efficient electron

[*] Dr. T. Tian, J. X. Zhong, M. Yang, W. Feng, Prof. W. Q. Wu
 MOE Key Laboratory of Bioinorganic and Synthetic Chemistry
 Lehn Institute of Functional Materials, School of Chemistry
 Sun Yat-sen University, Guangzhou 510006 (P. R. China)
 E-mail: wuwq36@mail.sysu.edu.cn



Prof. B. X. Lei
 School of Chemistry and Chemical Engineering, Key Laboratory of
 Electrochemical Energy Storage and Energy Conversion of Hainan
 Province, Hainan Normal University
 Haikou 571158 (P. R. China)
 E-mail: leibx@hainnu.edu.cn

C. Zhang, Prof. L. Wang
 Nanomaterials Centre, School of Chemical Engineering and
 Australian Institute for Bioengineering and Nanotechnology
 The University of Queensland, Brisbane, QLD 4072 (Australia)

E-mail: l.wang@uq.edu.au

Prof. Y. Abdi
 Nanophysics Research Laboratory, Department of Physics
 University of Tehran, P.O. Box 1439955961, Tehran (Iran)

Prof. W. Zhang
 Department of Environmental Engineering
 Technical University of Denmark (DTU)
 2800 Kgs. Lyngby (Denmark)

 Supporting information and the ORCID identification number(s) for the author(s) of this article can be found under:
 <https://doi.org/10.1002/anie.202108495>.

extraction at the ETL/perovskite interface. One does not need to concern about the high-temperature ($>450^{\circ}\text{C}$) sintering process and illumination-induced photocatalytic degradation of the perovskite like using conventional TiO_2 metal oxide ETL, which will raise the energy consumption during fabrication and incur hidden trouble of instability.^[17,20,23]

Given its exceptional optoelectronic properties, the C_{60} has been widely introduced as an interlayer between metal oxide ETL and perovskite layer to modify the interfacial carrier dynamics.^[24–26] Nonetheless, the PSCs only employing C_{60} as ETL have been rarely reported. Yang and co-workers reported depositing a compact C_{60} ETL via a thermal evaporation method,^[17,25,27] and a PCE of 15.20% has been achieved for all carbon-based PSCs. However, the versatility and up-scaling potential of using thermally evaporated C_{60} ETL would be possibly limited by the stringent requirement of using vacuum equipment and the complicated control over the deposition parameters.^[28] Fabricating the C_{60} layer via a solution process, for instance, by spin-coating or blade-coating, is simpler and thus more compatible to achieve high-throughput layer-by-layer coating of perovskite photovoltaic devices. But the solution-processed C_{60} ETL is normally not dense enough to ensure high carrier mobility and conductivity for extracting the photogenerated electrons efficiently. Worse still, the integrity of solution-processed C_{60} nanofilm is easily damaged by the solvent of perovskite ink, thus leading to current leakage or even short-circuiting of resultant devices. Above mentioned aspects have limited the research attempts and development of full solution-processed all carbon-based PSCs, not to mention the further advancement of the device

performance, especially the stability. Considering the bonding flexibility of C_{60} materials, it is highly desirable to chemically modify the TCO substrate, which could help to consolidate C_{60} deposition and then protect it from washing away by perovskite ink solvent.

In this study, we demonstrated a strategy to substantially improve the adhesion of the solution-processed C_{60} nanofilm on underlying indium tin oxide (ITO) substrate with the assist of a self-assembled monolayer of 3-aminopropyl triethoxysilane (APTES) that acts as a “molecular cement”. Via robust interfacial linkage engineering, the APTES molecules can toughen the ITO/ETL interface and preserve the integrity of C_{60} ETL upon perovskite layer deposition. We further fabricated a new class of all carbon-based PSCs (APTES-modified ITO/ C_{60} /perovskite/carbon) via a realistic full solution-based layer-by-layer blade-coating approach. The simplified PSCs without hole transport layer showcased a champion PCE of 18.6% with negligible $J-V$ hysteresis. Most encouragingly, the spontaneous self-encapsulation of perovskites with carbon-based electrodes significantly improved the lifespan of PSCs up to ca. 3000 hours without any PCEs loss in ambient conditions with a relative humidity of 30–50%.

We choose the APTES [$\text{H}_2\text{NCH}_2\text{CH}_2\text{CH}_2\text{Si}(\text{OC}_2\text{H}_5)_3$] triethoxysilane with $-\text{Si}(\text{OC}_2\text{H}_5)_3$ anchor group, $-\text{NH}_2$ terminal group, and $(\text{CH}_2)_n$ alkyl chain ($n=3$) as the chemical linker at ITO/ C_{60} interface, as shown in Figure 1a. The APTES was deposited on the ITO surface via blade-coating using the procedure described in the Experimental section in the Supporting Information (SI), followed by thermal treatment for consolidation and an ultrasonic cleaning process to

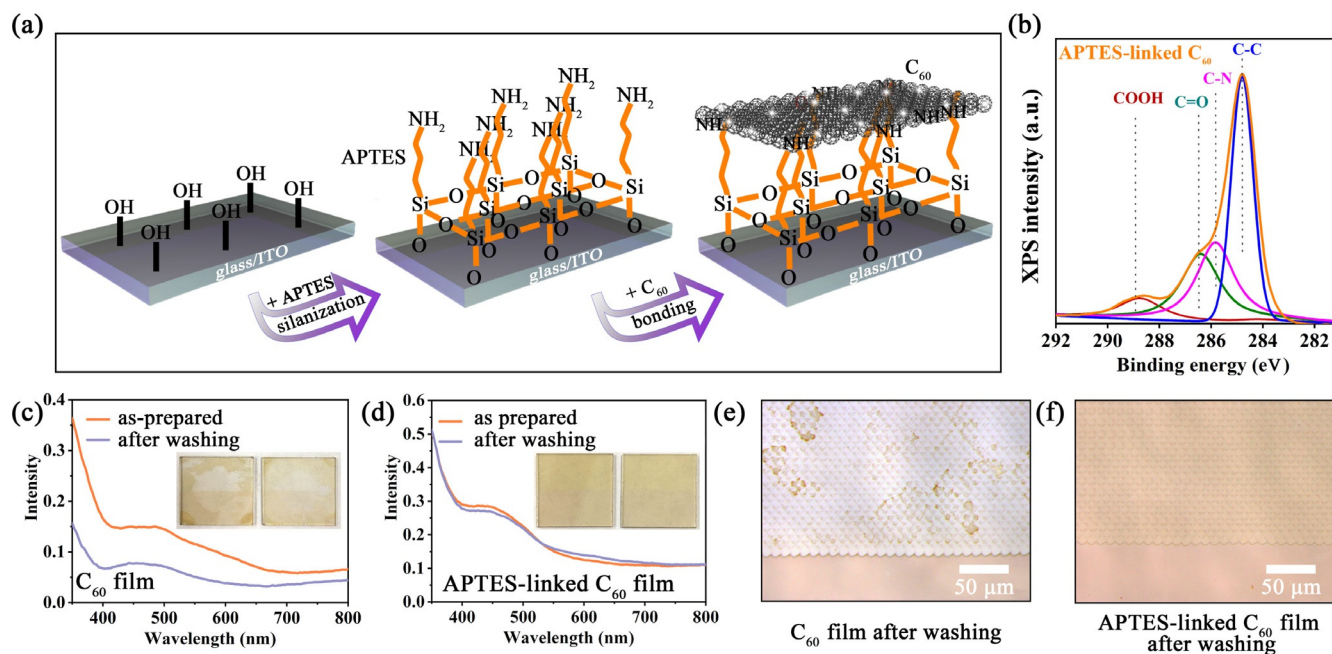


Figure 1. a) Illustration of the fabrication of APTES-linked C_{60} thin film on ITO glass substrate via a silanization and bonding process. b) The XPS spectra of the C 1s core levels of the C_{60} film with APTES treatment. The absorption spectra of c) the C_{60} film and d) APTES-linked C_{60} film deposited on the ITO glass substrate. Insets in c and d showed the real digital images of C_{60} and APTES-linked C_{60} films before (left) and after (right) DMF washing. The optical microscopy images of e) C_{60} film and f) APTES-linked C_{60} film after DMF washing. Note: the images were taken from the zoom-in area of the relevant films shown in the insets of (c) and (d).

remove the excessive molecules. It is noted that the APTES deposition is sensitive to several experimental parameters, including concentration, the solvent selected, aging conditions, blading speed, and temperature, etc. The beneficial roles of APTES linkers can be embodied in the following aspects. First, the surface of the ITO substrate is covered with -OH hydroxyl groups after the ultraviolet-ozone (UV-O₃) plasma treatment. In this case, the APTES could self-assemble and cross-link readily on -OH-modified ITO surfaces via a silanization process,^[29] forming a robust Si-O bonding environment. Second, the -NH₂ terminal group can chemically bond with C₆₀ thin film on top. It is worth pointing out the ETL fabrication was conducted in ambient condition, and specifically, the C₆₀/dichlorobenzene (DCB) solution was stirred for 2 hours at 150 °C, followed by an irradiation under white light for 48 hours in ambient air (see the details in the Experimental Section of the SI), resulting in the formation of highly reactive ¹O₂ species with excellent oxidizing capacity surround the C₆₀.^[30] This enabled the chemical interaction between APTES and light-activated C₆₀, which is beneficial to improve the adhesion strength of the C₆₀ ETL on the underlying ITO substrate.^[30,31] To our knowledge, such a mild phototreatment condition is not easy to induce the photopolymerization of C₆₀.^[32] Third, it is expected that only partial amounts of APTES bonded with C₆₀ or hydrolyzed, which makes the APTES-anchored surface sufficiently lyophilic for subsequent solution coating of the C₆₀ thin film with improved surface coverage. Fourth, the short alkyl chain length ($n = 3$) ensures an appropriate thickness of self-assemble APTES monolayer at a nanoscale level (ca. 1.3 nm, Figure S1), which could act as a charge tunneling contact to facilitate the interfacial charge extraction.^[33] Theoretically, it is possible to self-assemble another kinds of silane interlayer with shorter alkyl chain, which could further reduce the interfacial resistance at the C₆₀/ITO interface. However, one should also consider to correlate the alkyl chain length and packing density of insulating silanes to the effectiveness of forming a continuous interfacial charge tunneling contact.

Without APTES treatment, the C₆₀ has poor surface coverage on the ITO surface. In contrast, APTES anchoring enables a highly uniform coating of C₆₀ thin film on ITO substrate. The ITO/C₆₀ film demonstrated nearly the same transmittance as bare ITO from 550 to 800 nm, and it decreased less than 5 % compared with bare ITO from 350 nm to 550 nm owing to the absorbance of C₆₀ (Figure S2). Since the APTES improves the uniformity, coverage and adhesion of C₆₀ on the ITO substrate, the transmittance of APTES-modified ITO/C₆₀ film is slightly lower than ITO/C₆₀ film, especially at those adsorption regions of C₆₀. Considering the perovskite materials have a strong light adsorption capability from UV/Vis to near-infrared regions, such a small transmittance difference would not cause a substantial impact on the performance of resultant PSCs. To confirm the chemical interaction between APTES and C₆₀, the X-ray photoelectron spectroscopy (XPS) characterization has been conducted (Figure 1b). There are three XPS signals related to the C 1s of the C₆₀. For instance, the main peak at 284.7 eV can be indexed to the C-C bond, indicating most of the C atoms in C₆₀ are arranged within a conjugated honeycomb

lattice.^[28,34] The other two small peaks at 286.5 eV and 287.7 eV can be attributed to the bonding structures of C=O and C=O-O, respectively, which was similar to the observation reported elsewhere.^[25] A unique peak signal at 285.9 eV corresponded to the C-N bond was clearly observed in the APTES-linked C₆₀, suggesting the possible molecular interaction between APTES and C₆₀. In addition, the presence of N on the APTES-incorporated C₆₀, further validating the existence of APTES that could bond with C₆₀, rather than escaping away during thermal annealing of C₆₀ thin film (Figure S3).

The perovskite precursor normally employed polar solvents like dimethylformamide (DMF), dimethylsulfoxide (DMSO), or a combination of both. Unfortunately, we found that the solution-processed C₆₀ nanofilms can be easily washed out or partially damaged by perovskite precursor solvent, which led to a very poor surface coverage of C₆₀ film on ITO substrate, with many voids observed (Figure 1c and e). In this case, the perovskite layer and/or other functional layers can directly contact the underlying ITO substrate, leading to undesirable current leakage and charge recombination, thus deteriorating the device performance. In contrast, with the assist of favorable interfacial linkage by APTES, the as-deposited C₆₀ film uniformly coated on the ITO glass could to a large extent preserve its integrity and uniformity even after DMF solvent washing (Figure 1d and f). Not just limited to link the adjacent C₆₀ monolayer, we speculated that some portion of free APTES molecules could be extracted and incorporated to the matrix of C₆₀ nanofilm during the solution deposition process, which also helped to consolidate the entire C₆₀ bulk film and made it intractable upon DMF washing. The smooth and uniform surface of the C₆₀ layer is beneficial for the formation of a high-quality perovskite layer and the construction of an intimate ETL/perovskite interface, thus improving the performance of PSCs.^[17] The absorption change of ITO/C₆₀ film with or without APTES linking upon DMF washing was compared by using an ultraviolet-visible (UV/Vis) spectrophotometer, the absorption intensity of ITO/APTES-linked C₆₀ almost did not change, while the absorption intensity of ITO/C₆₀ dramatically decreased (Figures 1c and d). This result again highlighted the outstanding capability of APTES in linking the C₆₀ and ITO like a glue, which established a feasible platform and solid foundation to achieve full solution-processed PSCs with high device performance.

We fabricated the PSCs using the successively blade-coated APTES and C₆₀ film as ETL, perovskite layer as the light-harvesting layer, and carbon electrode as CE (Figure S4, see the details in Experimental Section). The monolithic all carbon-based device featured a planar architecture of APTES-modified ITO/C₆₀/perovskite (PVK)/carbon (Figure 2a). It is worth pointing out this is the pioneer demonstration of fully-printed perovskite photovoltaics in ambient conditions without relying on the vacuum environment, perovskite ink drop-casting and infiltration technique and expensive noble metal electrode. The development and implementation of this technique showcase a great potential to make the fabrication of thin-film photovoltaics as fast as printing the newspaper/magazine. We chose the mixed cation

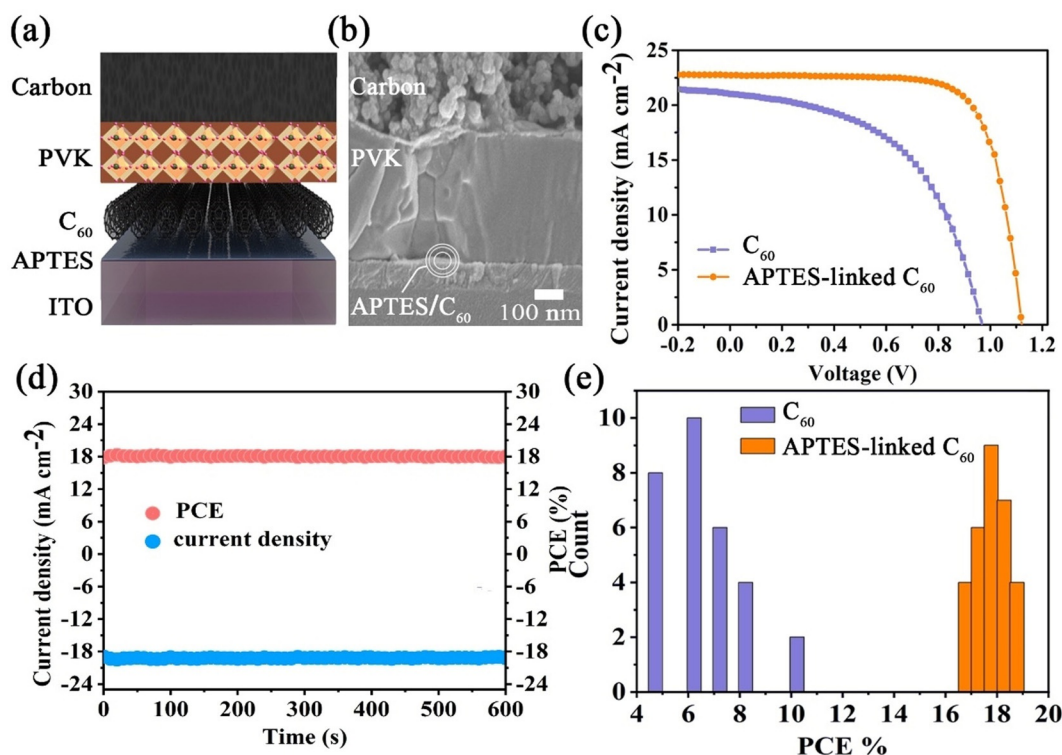


Figure 2. a) Illustration and b) cross-sectional SEM image of the all carbon-based PSC with a device architecture of ITO/APTES-linked C_{60} /PVK/carbon. c) J - V curves of the best-performing PSCs fabricated with C_{60} and APTES-linked C_{60} ETL. d) Stabilized current density and PCE at the maximum power point of 0.94 V for the champion device based on the APTES-linked C_{60} film. e) PCE histogram of the PSCs based on C_{60} films and APTES-linked C_{60} films.

perovskite composition, namely, $CS_{0.05}MA_{0.95}PbI_3$ (denoted as CM) with 1 mol% excess methylammonium iodide (MAI), optimized for high device performance, as it provides a favorable energy level alignment with other functional layers and exhibits improved thermal stability owing to the incorporation of cesium (Cs) cations.^[35,36] Figure 2b and S5 showed the all carbon-based PSC multilayer stack is composed of a ca. 18 nm-thick C_{60} film, a ca. 500 nm-thick CM perovskite layer, and a ca. 25 μ m-thick carbon electrode. Typically, the blade-coated CM perovskite film shows a columnar character with the grains monolithic throughout the film, forming intimate contacts with both ETL and CE. The carbon electrode with a vertical thickness of above 25 μ m can guarantee sufficient conductivity for collecting the charges and more importantly, form a natural “protection tent” on top of the perovskite layer to efficiently inhibit the water molecule ingress. Figure 2c shows the current density-voltage (J - V) characteristics of the best-performing all carbon-based PSCs with or without APTES treatment, and the corresponding photovoltaic parameters are summarized in Table 1.

The champion device fabricated with APTES-linked C_{60} ETL attained a high PCEs of 18.64%, which was 77% higher than of the control device without APTES treatment (10.52%). To the best of our knowledge, this is the record PCEs value for the carbon-electrode-based HTL-free PSCs, regardless of the perovskite compositions. The APTES treatment remarkably increased the short-circuit photocurrent density (J_{sc}) from 21.01 to 22.72 $mA\,cm^{-2}$, the open-circuit voltage (V_{oc}) from 0.98 V to 1.12 V, and the fill factor (FF)

from 0.51 to 0.73, and the resultant PSCs showed almost negligible J - V hysteresis (Figure S6 and Table S1). We attributed such a promising device performance enhancement to the reduced charge accumulation and improved electron extraction owing to a well-optimized TCO/ETL/perovskite interface with robust integrity and mechanical toughness.^[22,37,38] Specifically, the substantial V_{oc} enhancement can be attributed to the improved surface coverage of C_{60} ETL on APTES-treated ITO glass and the formation of charge tunneling contact via self-anchoring of APTES layer at TCO/ETL interface.^[33] It is worth pointing out the commonly demonstrated carbon electrode-based PSCs exhibited the FF lower than 70% owing to the under-optimized perovskite/carbon CE interface with inferior hole extraction and poor contact. Herein, we lifted the FF of the fully blade-coated all carbon-based PSCs to 73%, which can be affiliated with the fact that each functional layer is coated with desirable smoothness for optimizing contact junctions at relevant interfaces,^[39,40] and favorable p-doping of perovskite layer with excessive MAI for better hole extraction even in the

Table 1: Photovoltaic parameters of the PSCs based on CM perovskite films deposited on ITO/ C_{60} and ITO/APTES-linked C_{60} ETL substrates.^[a]

PSCs	J_{sc} [$mA\,cm^{-2}$]	V_{oc} [V]	η [%]	Average η [%]	FF
C_{60}	21.01	0.98	10.52	7.63 ± 2.89	0.51
APTES-Linked C_{60}	22.72	1.12	18.64	17.56 ± 1.08	0.73

[a] The average PCE was evaluated from a batch of 30 cells.

absence of hole transport layer.^[6,41] Further improvement of the device performance can be expected if the contact of the perovskite/carbon CE interface can be further optimized. The stabilized current and PCE output was recorded at a maximum power point of 0.94 V for the champion device, which steadied within seconds, giving a stabilized power output of 18.1 % under AM 1.5 G one-sun illumination (Figure 2d) and verifying the PCE values from the *J*-*V* curves. The PCE histogram of all carbon-based PSCs with or without APTES treatment was presented in Figure 2e, in which the data was collected from a batch of 30 devices for each condition. Specifically, more than 86 % of targeted devices with APTES treatment had PCE above 17 %, while only about 7 % of the control counterparts showed efficiencies over 10 %. This result highlights the effectiveness and significance of APTES-assisted interfacial bridging on improving the adhesion and integrity of C₆₀ ETL on TCO substrate, which led to high device performance, accompanied by a considerably improved reproducibility for the perovskite photovoltaics even fabricated via full solution-coating, thus providing a convincing promise towards future high throughput production and commercialization.^[5]

To better understand the beneficial roles of APTES interfacial linkage on improving the device performances of

all carbon-based PSCs, we carried out a series of optical, photoelectric and electrochemical characterizations for the perovskite films deposited on different substrates. Specifically, the steady-state photoluminescence (PL) measurement was performed to provide insight into interfacial carrier dynamics. Notably, for the CM perovskite film deposited on the APTES-linked C₆₀ film, a stronger PL quenching effect has been observed, as compared to the C₆₀ counterpart without any interfacial treatment (Figure S7), suggesting more efficient electron injection and transportation from CM perovskite to APTES-linked C₆₀ ETL upon 450 nm laser excitation.

The photo-excited charge transfer process at interfaces within PSCs was known to occur on a timescale of picoseconds, which significantly affects charge extraction and collection.^[33,42] The femtosecond (fs) transient absorption (TA) spectroscopy was applied to characterize the ultrafast carrier dynamic of the multilayer stack with the perovskite film deposited on top of C₆₀ ETL (Figure 3a). The contour plot of the TA spectrum of both C₆₀/CM and APTES-linked C₆₀/CM samples exhibited distinct ground-state bleaching (GSB) peak at ca. 750 nm, and its intensity can reflect the photoinduced carrier population in the conduction and valence bands of perovskite.^[33,43] In contrast to the control

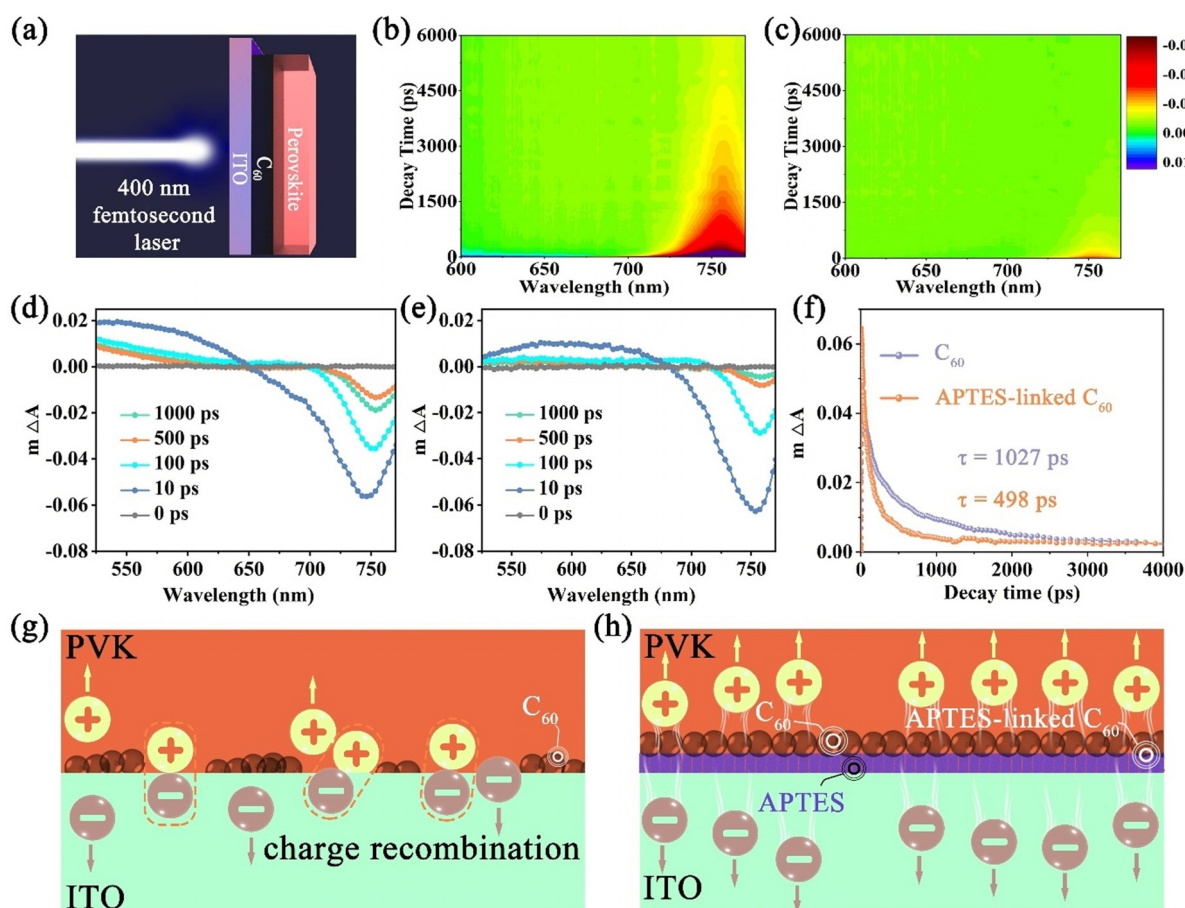


Figure 3. a) The layer-stacking structure for the TA measurement, where a 400 nm pump pulse generated by a fs-laser was used to probe the TA signal. b)–e) The contour plot and delay time-dependent TA spectrum of (b, d) C₆₀/CM and (c, e) APTES-Linked C₆₀/CM samples. f) Dynamic TA decay probed at the GSB peak for the samples with or without APTES interfacial linkage. Illustration of charge extraction and recombination at (g) C₆₀/CM and (h) APTES-linked C₆₀/CM interfaces.

C₆₀/CM sample (Figure 3b), a more promptly faded signal has been observed in the contour plot of the APTES-linked C₆₀/CM sample (Figure 3c), suggesting the photogenerated electrons were more efficiently extracted out to the ETL. The induced absorption change (ΔA) intensity of the GSB signal gradually decreased with prolonging delay time, and the GSB peak intensity at the same delay time of the perovskite film deposited on APTES-linked C₆₀ appeared to be much weaker (Figure 3d and e). Note the positive photoinduced absorption centered at ca. 600 nm is possibly related to the presence of dual valence band structure in CM perovskite, and the spectral shift is possibly owing to the optical transitions induced by occupancy and filling of the CM perovskite band-edge states upon fs-laser excitation.^[44] Accordingly, the decay kinetics of the GSB were analyzed and interpreted, which showed a much faster decay for the APTES-linked C₆₀/CM sample than that of the control C₆₀/CM (i.e., 498 ps versus 1027 ps, Figure 3f and Table S2). This result verified the great advantages of APTES interfacial linkage on accelerating electron extraction and collection through an ultrafast shuttle from perovskite to the TCO owing to the intimate ETL/perovskite contact junction and the presence of tunneling junction at the TCO/ETL interface, while the perovskite layer deposited on discontinuous C₆₀ island without APTES bonding would inevitably incur interfacial electron-hole recombination, thus impairing the device performance (see Figure 3g and h).

To better understand the carrier dynamic modulation function of APTES interlayer, we carried out a systematic study by optimizing the treatment concentrations of APTES/methanol solutions (i.e. 0.5 %, 2 %, 5 % and 10 % in volume ratio) and evaluated their influence on the final device performances. It was shown that 5 % volume ratio is the optimal condition to achieve the highest photovoltaic performance of resultant PSC (Figure S8). Too low APTES concentration is not capable to form condense and continuous tunneling contact, while too high APTES concentration will result in self-assembled thick APTES layer that would inevitably increase the charge transfer resistance at the TCO/ETL interface owing to the insulating property of APTES molecules.

Electrochemical impedance spectroscopy (EIS) was used to further investigate the charge recombination behaviors within the devices. The depicted Nyquist plots of all carbon-based PSCs were measured under the dark condition at an applied bias voltage of 0.9 V. Accordingly, the recombination resistance (R_{rec}) was calculated by fitting the EIS spectra with an equivalent circuit model (inset in Figure S9).^[45] As a result, the R_{rec} for the device based on APTES-linked C₆₀ is 950 Ω , which is larger than that of the control device based on the pristine C₆₀ without any modification (361 Ω). This result implied the role of APTES interfacial modification in suppressing the interfacial carrier recombination, which can be attributed to the aforementioned facilitated charge extraction at both the TCO/ETL and ETL/perovskite interfaces, as well as the effective passivation of trap states and thus the reduced trap-assisted recombination at the ETL/perovskite interface with intact fullerene coating.^[25,26] Overall, the well-optimized interfacial carrier dynamics, namely,

boosted charge collection and suppressed charge recombination induced by APTES interfacial linkage is advantageous for improving the performance of all carbon-based PSCs in an omnibearing manner.

Finally, we investigated the ambient and operational stability of all carbon-based PSCs without encapsulation. For the operational stability of the PSCs without encapsulation and external cooling, the APTES-linked C₆₀-based full cells retained 94 % of their original PCEs after continuous illumination for 500 hours in ambient condition, while the control devices only preserved 45 % of their initial PCEs during the same illumination duration (Figure 4a). The prolonged operational stability of the APTES-linked C₆₀-based PSCs can be attributed to the strengthened toughness of the TCO/ETL interface and the intact ETL/perovskite contact junction with APTES interfacial linkage, which could expedite the electron extraction and collection, while simultaneously reduce the interfacial charge accumulation and alleviate the undesirable charge recombination that occurred in the low-lying island if that region is not fully covered by fullerene. Then, we traced the changes of the photovoltaic performances of the unencapsulated PSC based on APTES-linked C₆₀ ETL. The device was stored in ambient condition with a relative humidity of 30–50 % at room temperature in the dark (Figure 4b). All the photovoltaic parameters slightly increased during the first 200 hours, which can be attributed to the gradual evaporation of the solvent in the carbon electrode for improved conductivity as well as residual perovskite crystallization process for improved film quality with less defects,^[46–49] thus achieving better charge transport and suppressed non-radiative recombination. Encouragingly, the PSCs based on APTES-linked C₆₀ and carbon electrode were shown to be very stable without any loss of initial efficiency after 3000 hours, consistently showing high PCEs over 18 %. As compared to the state-of-the-art conventional PSCs fabricated with the metal electrode and sophisticated encapsulation procedures, we attributed the extended lifespan of the targeted PSCs with all-carbon electrodes to the following effects of the APTES-assisted interfacial linkage and spontaneous carbon encapsulation. First, the carbon materials, especially for the carbon black and graphite-based electrodes, which are naturally hydrophobic, can serve as a robust “protection tent” to prevent the water ingress and penetration from incurring perovskite decomposition.^[21,50] Second, it is well-known that the continuous operation of full cells will inevitably increase the device temperature up to 60 °C, which imposes a great challenge towards employing perovskite photovoltaics in realistic working conditions, especially in summer hot days. Obviously, our demonstrated PSC with all carbon-based ETL and CE withstand to work under elevated temperature and humid environment owing to the excellent heat dissipation and water repellent capability of carbon materials (Figure 4c).^[51,52] Third, under operational conditions with abundant photo-generated charges and a built-in electric field, the presence of high concentrations of mobile ions and/or vacancies defects in perovskites would result in undesirable photocarrier recombination, thus degrading the device performance.^[43] In this work, the carbon materials and electrodes are chemically inert to the ion

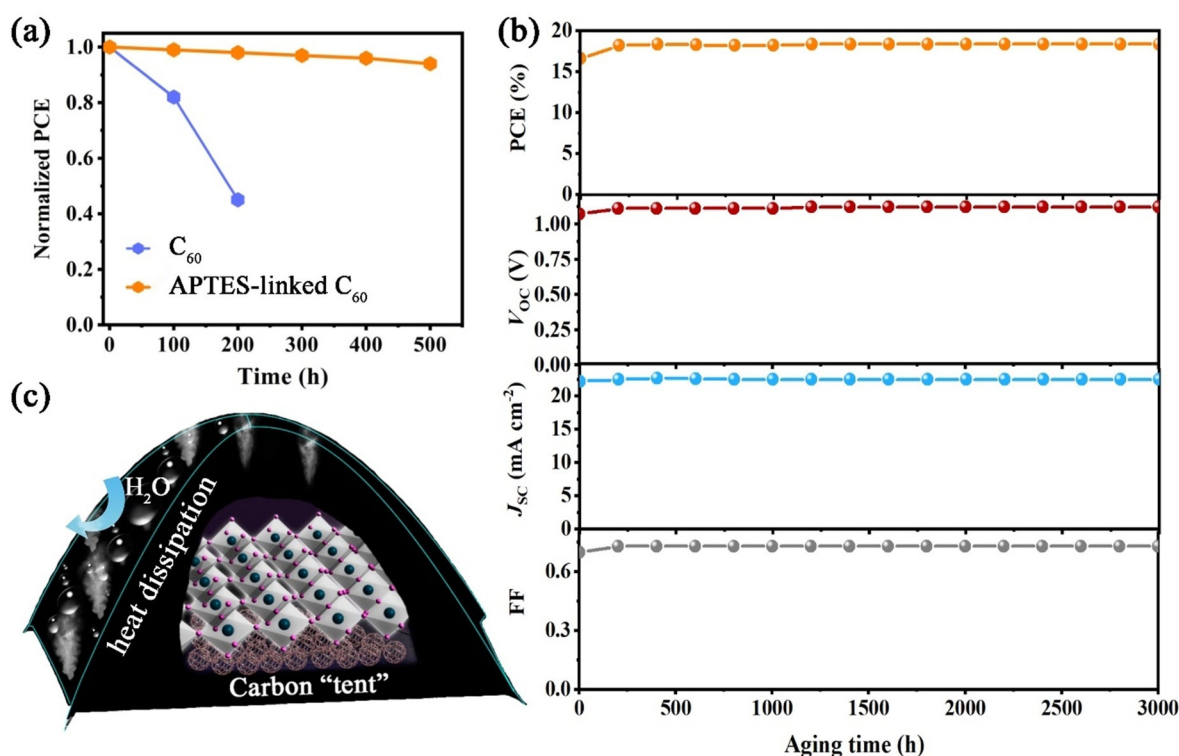


Figure 4. a) Operational stability of the unencapsulated PSCs fabricated with or without APTES treatment under continuous one sun illumination. b) Track record of the photovoltaic performance (PCE, V_{oc} , J_{sc} , and FF) of the champion all carbon-based PSC based on APTES-linked C₆₀ ETL upon storage in ambient condition. c) Illustration of self-encapsulation of perovskite layer by carbon materials, in which the carbon electrode outer layer serves as a carbon tent that could repel the water molecule and lose heat.

migration, which to a large extent minimizes the ion diffusion-induced electrode corrosion, perovskite decomposition and device performance degradation.^[13,14]

Conclusion

We have successfully demonstrated a full solution-printing of PSCs with a simplified device structure of ITO/APTES-linked C₆₀/perovskite/carbon. The self-assembled monolayer of cross-linkable APTES molecules can realize the maximum impact on strengthening the adhesion and interconnection of C₆₀ thin films on ITO substrate via favorable chemical interaction and bonding. When the interface was robustly bridged, the solution-processed C₆₀ film with enhanced toughness can to a large extent preserve its integrity upon subsequent perovskite ink deposition, thus forming an intact and intimate ETL/perovskite contact junction for accelerating electron extraction and collection, as well as suppressing interfacial charge recombination. Benefited from multifaceted advantages, the fully-printed all carbon-based PSCs fabricated with APTES-linked C₆₀ ETL and low-cost carbon electrode acquired a champion PCE of 18.64% without observable $J-V$ hysteresis, which is remarkably superior to that of the control device based on solution-processed C₆₀ without silane anchoring and modification and being one of the most efficient carbon-based solar cells reported to date. Moreover, the self-encapsulated carbon-based devices exhib-

ited significantly prolonged lifespan under ambient storage, thermal stress and continuous light illumination condition, which retained nearly 100% of initial efficiency after 3000 hours without any traceable degradation. We expect the long-term stability of all carbon-based PSCs can be further improved by optimizing the perovskite compositions and developing advanced encapsulation techniques. The layer-by-layer blade-coating is a cost-efficient approach that is amenable to scale-up for batch and/or high-throughput manufacturing of diverse perovskite-based optoelectronic devices with a high-performance and warranted lifetime. The findings reported herein could lead to fully printed perovskite photovoltaics.

Acknowledgements

The authors acknowledge the financial support from the National Natural Science Foundation of China (22005355) and the Guangdong Basic and Applied Basic Research Foundation (2019A1515110770). B.X.L. acknowledges the financial support from the National Natural Science Foundation of China (21965013). L.W. acknowledges the financial support from ARC through its Discovery program.

Conflict of Interest

The authors declare no conflict of interest.

Keywords: blade-coating · carbon · charge extraction · interfacial modification · perovskite solar cells

- [1] B. Chen, P. N. Rudd, S. Yang, Y. Yuan, J. Huang, *Chem. Soc. Rev.* **2019**, *48*, 3842–3867.
- [2] G. E. Eperon, S. D. Stranks, C. Menelaou, M. B. Johnston, L. M. Herz, H. J. Snaith, *Energy Environ. Sci.* **2014**, *7*, 982–988.
- [3] N. J. Jeon, J. H. Noh, Y. C. Kim, W. S. Yang, S. Ryu, S. I. Seok, *Nat. Mater.* **2014**, *13*, 897–903.
- [4] D. Liu, T. L. Kelly, *Nat. Photonics* **2014**, *8*, 133–138.
- [5] X. Chen, Y. Xia, Q. Huang, Z. Li, A. Mei, Y. Hu, T. Wang, R. Cheacharoen, Y. Rong, H. Han, *Adv. Energy Mater.* **2021**, *11*, 2100292.
- [6] W.-Q. Wu, Q. Wang, Y. Fang, Y. Shao, S. Tang, Y. Deng, H. Lu, Y. Liu, T. Li, Z. Yang, A. Gruverman, J. Huang, *Nat. Commun.* **2018**, *9*, 1625.
- [7] J. Jeong, M. Kim, J. Seo, H. Lu, P. Ahlawat, A. Mishra, Y. Yang, M. A. Hope, F. T. Eickemeyer, M. Kim, Y. J. Yoon, I. W. Choi, B. P. Darwich, S. J. Choi, Y. Jo, J. H. Lee, B. Walker, S. M. Zakeeruddin, L. Emsley, U. Rothlisberger, A. Hagfeldt, D. S. Kim, M. Grätzel, J. Y. Kim, *Nature* **2021**, *592*, 381–385.
- [8] S. De Wolf, J. Holovsky, S. J. Moon, P. Lper, C. Ballif, *J. Phys. Chem. Lett.* **2014**, *5*, 1035–1039.
- [9] Best Research-Cell efficiency chart, <https://www.nrel.gov/pv/cell-efficiency.html>, accessed: March 2021.
- [10] D. Yang, R. Yang, S. Priya, S. Liu, *Angew. Chem. Int. Ed.* **2019**, *58*, 4466–4483; *Angew. Chem.* **2019**, *131*, 4512–4530.
- [11] L. Zhou, J.-F. Liao, Z.-G. Huang, J.-H. Wei, X.-D. Wang, W.-G. Li, H.-Y. Chen, D.-B. Kuang, C.-Y. Su, *Angew. Chem. Int. Ed.* **2019**, *58*, 5277–5281; *Angew. Chem.* **2019**, *131*, 5331–5335.
- [12] B. Chen, Z. J. Yu, S. Manzoor, S. Wang, W. Weigand, Z. Yu, G. Yang, Z. Ni, X. Dai, Z. C. Holman, J. Huang, *Joule* **2020**, *4*, 850–864.
- [13] A. K. Baranwal, S. Kanaya, T. Peiris, M. Gai, S. Ito, *ChemSusChem* **2016**, *9*, 2604–2608.
- [14] D. Bogachuk, S. Zouhair, K. Wojciechowski, B. Yang, V. Babu, L. Wagner, B. Xu, J. Lim, S. Mastroianni, H. Pettersson, A. Hagfeldt, A. Hinsch, *Energy Environ. Sci.* **2020**, *13*, 3880–3916.
- [15] C. Tian, S. Zhang, S. Li, A. Mei, D. Li, S. Liu, D. Zhang, Y. Hu, Y. Rong, H. Han, *Sol. RRL* **2018**, *2*, 1800174.
- [16] K. Domanski, J.-P. Correa-Baena, N. Mine, M. K. Nazeeruddin, A. Abate, M. Saliba, W. Tress, A. Hagfeldt, M. Grätzel, *ACS Nano* **2016**, *10*, 6306–6314.
- [17] X. Meng, J. Zhou, J. Hou, X. Tao, S. H. Cheung, S. K. So, S. Yang, *Adv. Mater.* **2018**, *30*, 1706975.
- [18] S. Gholipour, J. P. Correa-Baena, K. Domanski, T. Matsui, L. Steier, F. Giordano, F. Tajabadi, W. Tress, M. Saliba, A. A. bate, *Adv. Energy Mater.* **2016**, *6*, 1601116.
- [19] H. Azimi, T. Ameri, H. Zhang, Y. Hou, C. O. R. Quiroz, J. Min, M. Hu, Z.-G. Zhang, T. Przybilla, G. J. Matt, E. Spiecker, Y. Li, C. J. Brabec, *Adv. Energy Mater.* **2015**, *5*, 1401692.
- [20] R. He, X. Huang, M. Chee, F. Hao, P. Dong, *Carbon Energy* **2019**, *1*, 109–123.
- [21] Z. Yu, B. Chen, P. Liu, C. Wang, C. Bu, N. Cheng, S. Bai, Y. Yan, X. Zhao, *Adv. Energy Mater.* **2016**, *6*, 4866–4873.
- [22] P. Docampo, J. M. Ball, M. Darwich, G. E. Eperon, H. J. Snaith, *Nat. Commun.* **2013**, *4*, 2761.
- [23] Y. Li, K. Lu, X. Ling, J. Yuan, G. Shi, G. Ding, J. Sun, S. Shi, X. Gong, W. Ma, *J. Mater. Chem. A* **2016**, *4*, 10130–10134.
- [24] P.-W. Liang, C.-C. Chueh, S. T. Williams, A. K.-Y. Jen, *Adv. Energy Mater.* **2015**, *5*, 1402321.
- [25] J.-Y. Jeng, Y. F. Chiang, M. H. Lee, S. R. Peng, T. F. Guo, P. Chen, T. C. Wen, *Adv. Mater.* **2013**, *25*, 3727–3732.
- [26] D. Ouyang, J. Zheng, Z. Huang, L. Zhu, W. C. H. Choy, *J. Mater. Chem. A* **2021**, *9*, 371–379.
- [27] X. Zheng, B. Chen, J. Dai, Y. Fang, Y. Bai, Y. Lin, H. Wei, X. C. Zeng, J. Huang, *Nat. Energy* **2017**, *2*, 17102.
- [28] H. H. Jin, H. S. Dong, H. J. Min, M. L. Lee, H. I. Sang, *J. Mater. Chem. A* **2017**, *5*, 21146–21152.
- [29] M. R. Pugalenth, G. Cao, M. R. Prabhu, *Energy Fuels* **2020**, *34*, 10087–10099.
- [30] J. Lee, Y. Mackeyev, M. Cho, L. J. Wilson, J. H. Kim, P. J. J. Alvarez, *Environ. Sci. Technol.* **2010**, *44*, 9488–9495.
- [31] R. G. Acres, A. V. Ellis, J. Alvino, C. E. Lenahan, D. A. Khodakov, G. F. Metha, G. G. Andersson, *J. Mater. Chem. C* **2012**, *116*, 6289–6297.
- [32] A. M. Rao, P. Zhou, K.-A. Wang, G. T. Hager, J. M. Holden, Y. Wang, W.-T. Lee, X.-X. Bi, P. C. Eklund, D. S. Cornett, M. A. Duncan, I. J. Amster, *Science* **1993**, *259*, 955–957.
- [33] W.-Q. Wu, J.-X. Zhong, J.-F. Liao, C. Zhang, D.-B. Kuang, *Nano Energy* **2020**, *75*, 104929.
- [34] Y. Wang, Y. Shao, D. W. Matson, J. Li, Y. Lin, *ACS Nano* **2010**, *4*, 1790–1798.
- [35] M. Saliba, T. Matsui, J. Y. Seo, K. Domanski, J. P. Correa-Baena, M. K. Nazeeruddin, S. M. Zakeeruddin, W. Tress, A. Abate, A. Hagfeldt, M. Grätzel, *Energy Environ. Sci.* **2016**, *9*, 1989–1997.
- [36] T. Singh, T. Miyasaka, *Adv. Energy Mater.* **2018**, *8*, 1700677.
- [37] T. Xue, G. Chen, X. Hu, M. Su, Z. Huang, X. Meng, Z. Jin, J. Ma, Y. Zhang, Y. Song, *ACS Appl. Mater. Interfaces* **2021**, *13*, 19959–19969.
- [38] L. Zeng, S. Chen, K. Forberich, C. J. Brabec, Y. Mai, F. Guo, *Energy Environ. Sci.* **2020**, *13*, 4666–4690.
- [39] W.-Q. Wu, P. N. Rudd, Q. Wang, Z. Yang, J. Huang, *Adv. Mater.* **2020**, *32*, 2000995.
- [40] W.-Q. Wu, Z. Yang, P. N. Rudd, Y. Shao, X. Dai, H. Wei, J. Zhao, Y. Fang, Q. Wang, Y. Liu, *Sci. Adv.* **2019**, *5*, eaav8925.
- [41] J. Shi, Y. Li, Y. Li, D. Li, Y. Luo, H. Wu, Q. Meng, *Joule* **2018**, *2*, 879–901.
- [42] W.-Q. Wu, P. N. Rudd, Z. Ni, C. Brackley, J. Huang, *J. Am. Chem. Soc.* **2020**, *142*, 3989–3996.
- [43] J. P. Correa Baena, L. Steier, W. Tress, M. Saliba, S. Neutzner, T. Matsui, F. Giordano, T. J. Jacobsson, A. R. Srimath Kandada, S. M. Zakeeruddin, A. Petrozza, A. Abate, M. K. Nazeeruddin, M. Grätzel, A. Hagfeldt, *Energy Environ. Sci.* **2015**, *8*, 2928–2934.
- [44] J. S. Manser, P. V. Kamat, *Nat. Photonics* **2014**, *8*, 737–743.
- [45] Z. Wang, A. Ganose, C. Niu, D. O. Scanlon, *J. Mater. Chem. A* **2018**, *6*, 5652–5660.
- [46] W. A. Dunlap-Shohl, Y. Zhou, N. P. Padture, D. B. Mitzi, *Chem. Rev.* **2019**, *119*, 3193–3295.
- [47] M. Anaya, J. F. Galisteo-López, M. E. Calvo, C. López, H. Míguez, *J. Phys. Chem. C* **2016**, *120*, 3071–3076.
- [48] D. Bogachuk, L. Wagner, S. Mastroianni, M. Daub, H. Hillbrecht, A. Hinsch, *J. Mater. Chem. A* **2020**, *8*, 9788–9796.
- [49] L. Wagner, L. E. Mundt, G. Mathiazhagan, M. Mundus, M. C. Schubert, S. Mastroianni, U. Würfel, A. Hinsch, S. W. Glunz, *Sci. Rep.* **2017**, *7*, 14899.
- [50] G. Zhang, P. Xie, Z. Huang, Z. Yang, Z. Pan, Y. Fang, H. Rao, X. Zhong, *Adv. Funct. Mater.* **2021**, *31*, 2011187.
- [51] E. T. Thostenson, Z. Ren, T. W. Chou, *Compos. Sci. Technol.* **2001**, *61*, 1899–1912.
- [52] F. G. Emmerich, *Carbon* **2014**, *79*, 274–293.

Manuscript received: June 25, 2021

Revised manuscript received: August 11, 2021

Accepted manuscript online: August 19, 2021

Version of record online: September 21, 2021